crystals

MDPI

Article

Experimental Investigation and Machine Learning Modeling of Tribological Characteristics of AZ31/B_4C/GNPs Hybrid Composites

Dhanunjay Kumar Ammisetti [1], Bharat Kumar Chigilipalli [2], Baburao Gaddala [3], Ravi Kumar Kottala [4,*], Radhamanohar Aepuru [5], T. Srinivasa Rao [6], Seepana Praveenkumar [7,*] and Ravinder Kumar [8]

1 Department of Mechanical Engineering, Lakireddy Bali Reddy College of Engineering, Mylavaram 521230, Andhra Pradesh, India; adkphdnitt@gmail.com
2 Department of Mechanical Engineering, Vignan's Institute of Information Technology (A), Visakhapatnam 530049, Andhra Pradesh, India; chbharat334@gmail.com
3 Mechanical and Industrial Engineering Section, Chemical Engineering Specialization, University of Technology and Applied Sciences Muscat, Alkhuwair, P.O. Box 74, Muscat 133, Oman; baburao01803@gmail.com
4 Department of Mechanical Engineering, M V G R College of Engineering (A), Vizianagaram 535005, Andhra Pradesh, India
5 Departamento de Mecánica, Facultad de Ingeniería, Universidad Tecnológica Metropolitana, Santiago 7800002, Chile; raepuru@utem.cl
6 Department of Mechanical Engineering, Vasireddy Venkatadri Institute of Technology, Nambur 522508, Andhra Pradesh, India; sr.tanneeru@gmail.com
7 Department of Nuclear and Renewable Energy Sources, Ural Federal University, Yekaterinburg City 620002, Russia
8 Department of Mechanical Engineering, Lovely Professional University, Phagwara 144411, Punjab, India; rav.chauhan@yahoo.co.in
* Correspondence: kottalaravikumar15@gmail.com (R.K.K.); seepanapraveenkumar5@gmail.com (S.P.)

check for updates

Citation: Ammisetti, D.K.; Chigilipalli, B.K.; Gaddala, B.; Kottala, R.K.; Aepuru, R.; Rao, T.S.; Praveenkumar, S.; Kumar, R. Experimental Investigation and Machine Learning Modeling of Tribological Characteristics of AZ31/B_4C/GNPs Hybrid Composites. *Crystals* **2024**, *14*, 1007. https://doi.org/10.3390/cryst14121007

Academic Editor: Liangchi Zhang

Received: 17 October 2024
Revised: 16 November 2024
Accepted: 19 November 2024
Published: 21 November 2024

Copyright: © 2024 by the authors. Licensee MDPI, Basel, Switzerland. This article is an open access article distributed under the terms and conditions of the Creative Commons Attribution (CC BY) license (https://creativecommons.org/licenses/by/4.0/).

Abstract: In this study, the AZ31 hybrid composites reinforced with boron carbide (B_4C) and graphene nano-platelets (GNPs) are prepared by the stir casting method. The main aim of the study is to study the effect of various wear parameters (reinforcement percentage (R), applied load (L), sliding distance (D), and velocity (V)) on the wear characteristics (wear rate (WR)) of the AZ91/B_4C/GNP composites. Experiments are designed using the Taguchi technique, and it was determined that load (L) is the most significant parameter affecting WR, followed by D, R, and V. The wear mechanisms under conditions of maximum and minimum wear rates are examined using SEM analysis of the worn-out surfaces of the specimens. From the result analysis on the WR, the ideal conditions for achieving the lowest WR are R = 4 wt.%, L = 15 N, V = 3 m/s, and D = 500 m. Machine learning (ML) models, including linear regression (LR), polynomial regression (PR), random forest (RF), and Gaussian process regression (GPR), are implemented to develop a reliable prediction model that forecasts output responses in accordance with input variables. A total of 90% of the experimental data points were used to train and 10% to evaluate the models. The PR model exceeded the accuracy of other models in predicting WR, with R^2 = 0.953, MSE = 0.011, RMSE = 0.103, and COF with R^2 = 0.937, MSE = 0.013, and RMSE = 0.114, respectively.

Keywords: magnesium; stir casting; hybrid composites; wear rate (WR); coefficient of friction (COF); machine learning

1. Introduction

In recent times, industries and researchers have been motivated to concentrate on lightweight, high-performance materials due to the frequent changes in societal and environmental requirements, as well as the evolving legal constraints on vehicle specifications and traffic rules. Due to their superior machinability, recyclability, damping capacity, and

low density, magnesium (Mg) and its alloys have recently become a popular choice in the aerospace, automotive, and electronics industries [1–3]. However, the use of magnesium is restricted due to its lack of strength, inadequate ability to resist corrosion, and low resistance to wear [4]. In order to address these constraints, many researchers have integrated various enhancements such as B_4C, silicon carbides (SiC), aluminum oxide Al_2O_3, graphene, etc. [5–10] with the aim of developing a magnesium composite material. AZ31 is a frequently employed magnesium alloy in the production of structural components for automotive products and aerospace. Furthermore, it has been determined that wear is a significant issue faced by automotive elements. Varaprasad et al. [11] conducted a study to investigate the impact of Al_2O_3 on the wear characteristics of AZ31 composites. The experiments were carried out at various velocities, pressures, and distances. The study revealed a negative correlation between the wt.% of Al_2O_3 in the composite and the wear rate (WR), indicating that a rise in the former leads to a decrease in the latter. In addition, the friction coefficient dropped as the load increased, whereas distance and velocity had a minimal effect. Kartheesan et al. [12] examined the impact of CaO concentration, velocity (V), load (L), and distance (D) on the friction and wear properties of Mg/CaO composites. The results of this investigation suggest that an increase in the speed results in a decrease in the composites' WR. The presence of the oxide film on the pin's surface is the underlying cause of this phenomenon. Abebe et al. [13] assessed the influence of wear metrics (V, L, and D) on the wear characteristics of AZ61/ZrO_2/SiC composites, which were developed through friction stir consolidation (FSC). Finally, their research demonstrated the effectiveness of both the Genetic Algorithm (GA) and Response Surface Methodology (RSM) methods in improving the wear behavior of the MMCs that were produced via the FSC technique. Mahdi et al. [14] investigated the role of reinforcement particle size and morphology in the tribological characteristics and hardness of AZ31 Mg alloy composites. Friction stir processing (FSP) was employed to fabricate mono and hybrid composites using ceramic reinforcements, such as boron carbide (B_4C, 150 µm), tungsten carbide (WC, 5 µm), and zirconia (ZrO_2, 35 nm). The particle distribution was homogenous in the SEM. The AZ31/ZrO_2 nanocomposite exhibited a 120% increase in hardness, while AZ31/B_4C exhibited the maximum wear resistance and the lowest friction coefficient. SEM revealed abrasive wear mechanisms, and hybrid composites enhanced friction performance and wear resistance. Thoufiq et al. [15] conducted a study with the objective of fabricating, mechanically analyzing, and assessing the dry sliding wear properties of AZ31 Mg alloy composites enhanced with TiO_2 and Sn. AZ31/TiO_2 composites with different wt.% of TiO_2 (0.5%, 1.5%, and 2.5%) were created. Additionally, hybrid AZ31/1.5 wt.% TiO_2 composites were further strengthened with varying wt.% of Sn (3%, 6%, 9%, and 12%). The microstructural study revealed a homogeneous dispersion of reinforcing particles. Through mechanical testing, it was shown that the tensile strength, microhardness, and compressive properties experienced enhancement up to a concentration of 1.5 wt.% TiO_2 and 6 wt.% Sn. However, beyond this concentration, the qualities started to deteriorate. Wear experiments were performed on three different materials: AZ31 alloy, AZ31/1.5TiO_2 composite, and hybrid composites. The tests were conducted using a pin-on-disk tribometer, with normal loads ranging from 10 N to 40 N, a sliding speed of 0.5 m/s, and a total distance of 1000 m. The hybrid composite containing 6 wt.% of Sn demonstrated superior mechanical and wear characteristics. The application of FESEM and EDS in morphological analysis revealed that abrasion, adhesion, and delamination are the primary wear mechanisms.

Metal matrix composites (MMCs) are sophisticated materials consisting of a metal or alloy matrix reinforced with ceramic, metallic, or other fibers and particles to improve particular qualities. By including reinforcing materials such as silicon carbide, alumina, or carbon fibers, metal matrix composites (MMCs) attain a distinctive amalgamation of strength, stiffness, and lightweight characteristics, rendering them very advantageous in rigorous applications. MMCs are extensively utilized in aerospace, automotive, and military sectors due to their exceptional strength-to-weight ratios and resistance to wear, corrosion, and thermal expansion, which provide considerable performance advantages. Moreover,

MMCs can be customized to fulfill certain engineering specifications by modifying the kind, size, and distribution of reinforcement within the matrix, hence providing enhanced adaptability compared to conventional metals. Nonetheless, the intricacy of manufacturing processes and elevated costs continue to present hurdles, but continuing research seeks to enhance the cost-effectiveness and usability of MMCs across diverse industries. In this specific MMC, AZ31 magnesium alloy functions as the matrix material. AZ31 is a magnesium alloy characterized by a high strength-to-weight ratio, corrosion resistance, and advantageous mechanical properties, rendering it ideal for applications requiring weight reduction, including aerospace, automotive, and lightweight structural uses. The selection of AZ31 as the matrix capitalizes on magnesium's favorable machinability and recyclability, which aligns with contemporary sustainable design principles. This MMC incorporates boron carbide (B_4C) and graphene as reinforcements. Boron carbide is a highly durable ceramic characterized by significant thermal stability, exceptional hardness, and superior wear resistance, which enhances the composite's overall hardness, impact resistance, and structural integrity. This renders it an optimal reinforcement material, particularly in applications subjected to significant wear or necessitating enhanced hardness. Conversely, graphene, a carbon-derived nanomaterial, contributes a variety of distinctive properties to the composite. Graphene is recognized for its remarkable mechanical strength, thermal conductivity, and electrical properties, which improve the composite's tensile strength, flexibility, and thermal conductivity. Boron carbide and graphene synergistically enhance the AZ31 matrix, resulting in a composite that achieves a balance of lightweight strength, durability, and multifunctional performance characteristics. The composite is fabricated using stir casting, a widely utilized and economical method for producing metal matrix composites. In stir casting, reinforcements are mechanically incorporated into the molten metal matrix, facilitating a more uniform distribution of particles within the matrix material. This method facilitates precise control over the volume fraction of reinforcements, offers scalability, and is especially effective for the production of bulk quantities of metal matrix composites (MMCs). Challenges including the clustering of reinforcements, achieving uniform dispersion, and managing process parameters to prevent oxidation or degradation of both the matrix and reinforcements are essential considerations. The application of stir casting for the incorporation of boron carbide and graphene into an AZ31 matrix exemplifies an effective method for producing a composite characterized by enhanced structural integrity and customized properties for advanced applications.

The literature available suggests that the wear rate (WR) and friction of composite materials are greatly affected by parameters such as sliding speed, normal load, and sliding distance. Conducting experiments is indispensable for understanding the effects of these factors in various contexts. It is frequently difficult to conduct all of the requisite evaluations due to practical constraints, such as limited resources. In order to surmount this obstacle, it is possible to generate precise predictions of outcomes through the implementation of effective computational models. Due to recent developments in computational science, a variety of prediction techniques, including decision tree (DT) and random forest (RF), have been implemented to examine the impact of V, L, and D on wear characteristics without the necessity of conducting intensive experimentation. Aydin et al. [16] investigated the use of machine learning (ML) models to forecast the wear rate of AZ91 alloy, a magnesium-based alloy known for its lightweight and high mechanical qualities. The researchers used ML models such as Support Vector Machine (SVM), random forest (RF), and Artificial Neural Networks (ANN) to assess wear rate under diverse scenarios. These models were trained using a dataset of experimental wear tests, and their predictive accuracy was measured by comparing anticipated wear rates to actual experimental data. Aydin et al. [16] discovered that the ANN model produced the best accurate predictions, with a correlation coefficient (R^2) of 0.9845. This high result suggested that the ANN-predicted wear rates agreed well with the experimentally obtained data. ANN's improved performance has been attributed to its capacity to capture complicated, nonlinear correlations between input parameters (such as load, sliding speed, and material qualities) and wear rate. In contrast, while

SVM and RF models were useful, they did not achieve the same degree of accuracy as the ANN. The work emphasizes the potential of machine learning approaches, specifically ANN, in improving the prediction of wear rates in engineering materials such as AZ91 alloy, which can aid in material design and reduce the need for extensive experimental testing. Vara prasad et al. [17] conducted a study to examine the wear properties of an Mg composite reinforced with BN using ANN. The objective was to create a dependable predictive model for accurately forecasting the precise wear rate of the Mg/BN composite, which is essential for enhancing material performance in the real world. In order to accomplish this, the researchers devised an ANN model with a 3-5-1 architecture. The input nodes represent the variables that impact wear characteristics, including L, D, and V. The hidden layer, consisting of five nodes, processes the inputs in order to capture intricate and nonlinear relationships. The sole output node delivers the anticipated precise wear rate of the composite. The model was trained using empirical data obtained from wear tests conducted on the Mg/BN composite. After being trained, the ANN model was utilized to forecast the precise rate at which wear occurs under different circumstances. The predictions were subsequently compared to the actual experimental results in order to assess the accuracy of the model. The results demonstrated that the ANN model accurately predicted the precise wear rate with a remarkable level of precision, attaining an average deviation of only 2.6%. The minimal error margin indicates that the model's predictions are closely aligned with the experimental data, showcasing its efficacy in forecasting wear characteristics without the need for substantial supplementary testing. The efficacy of the ANN model underscores its promise as a valuable instrument for material design and performance optimization in engineering applications.

The available literature indicates that there is a scarcity of studies investigating the wear properties of AZ31 hybrid composites containing B_4C and GNPs. There is still a limited understanding of how various wear parameters, such as D, L, and V, affect the wear behavior of B_4C and GNP-reinforced AZ31 composites. Therefore, this work aims to understand the impact of different wear parameters on the wear characteristics displayed by AZ31 composites, including B_4C and GNPs. Additionally, it is evident from the existing literature that machine learning models, such as linear regression (LR), polynomial regression (PR), random forests (RF), and Gaussian process regression (GPR), have proven to be successful and widely used in predicting the wear features of composite materials. Thus, LR, PR, RF, and GPR models were utilized to analyze the wear nature of AZ31 composites reinforced with B_4C and GNPs, resulting in precise predictions.

2. Materials and Methods

Figure 1 depicts the flow chart of the present work. The materials used in the construction of the experimental rig and the various equipment used in recording the experimental data are presented in this section.

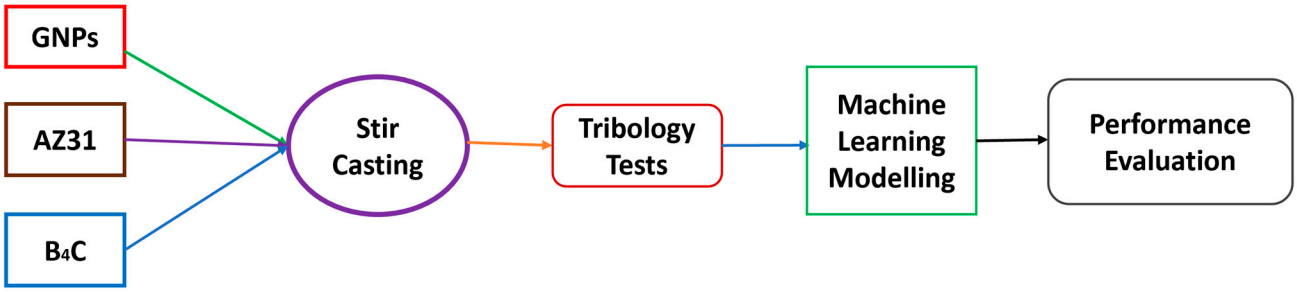


Figure 1. Flow chart.

2.1. Fabrication of Composites

The AZ31 alloy is employed as a matrix in the current study with the objective of generating hybrid composites. These composites are reinforced with boron carbide (B_4C) and

graphene nano-platelets (GNPs). The chemical components of AZ31 are illustrated in Table 1. The reinforcements are illustrated in Figure 2a,b through SEM images. Figure 2c,d depicts the EDS analysis and elements in the reinforcements. Figure 2e,f represents the XRD analysis of the GNPs and B_4C respectively. The inert gas-assisted stir casting technique is employed to produce hybrid composites, which are composed of varying proportions of reinforcements. In order to dissolve AZ91 ingots, the furnace is upheld at a temperature of 750 °C. A vortex is created by employing a stirrer to generate a rotating motion. Subsequently, the hot nano-powder was incorporated into the melted substance once the furnace's temperature reached the significant threshold of 750 °C. In order to ensure that the reinforcing elements were uniformly incorporated, stirring was performed at a rate of 400 rpm for a period of 15 min. A controlled gaseous condition consisting of a mixture of argon and SF_6 was meticulously maintained throughout the experimental procedure to prevent the oxidation of AZ31. The wt.% of GNPs in the hybrid composites was kept at an unchanged level of 1 wt.%, while the wt.% of the other component was altered between 1 wt.% and 3 wt.%. In order to mitigate the adverse effects of higher percentages of nano-reinforcements, such as insufficient blending and clustering within the composite, the concentrations of GNPs and the total concentration of reinforcements were restricted to 1% and 4%, respectively. Table 2 contains the specifications of the composites.

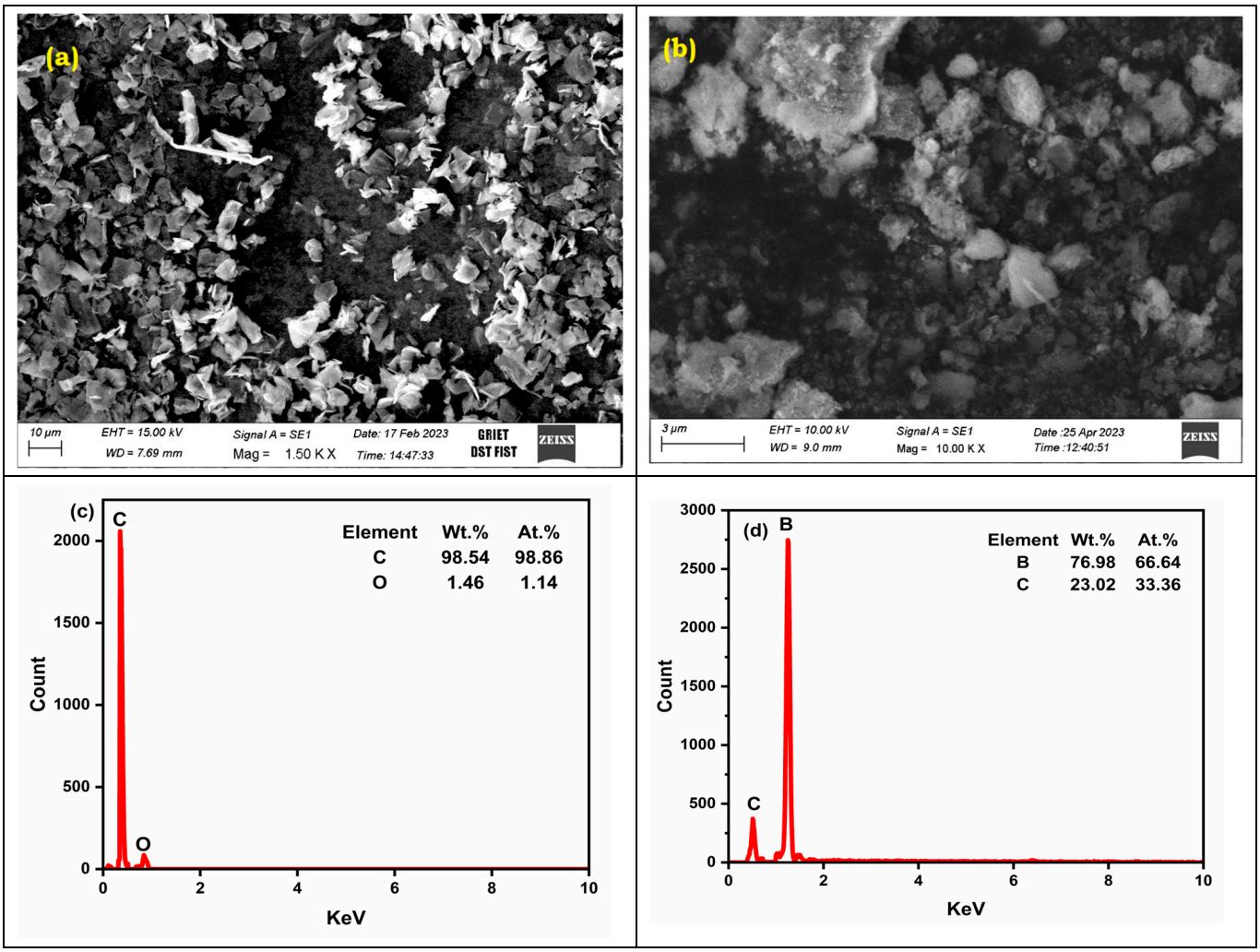


Figure 2. *Cont.*

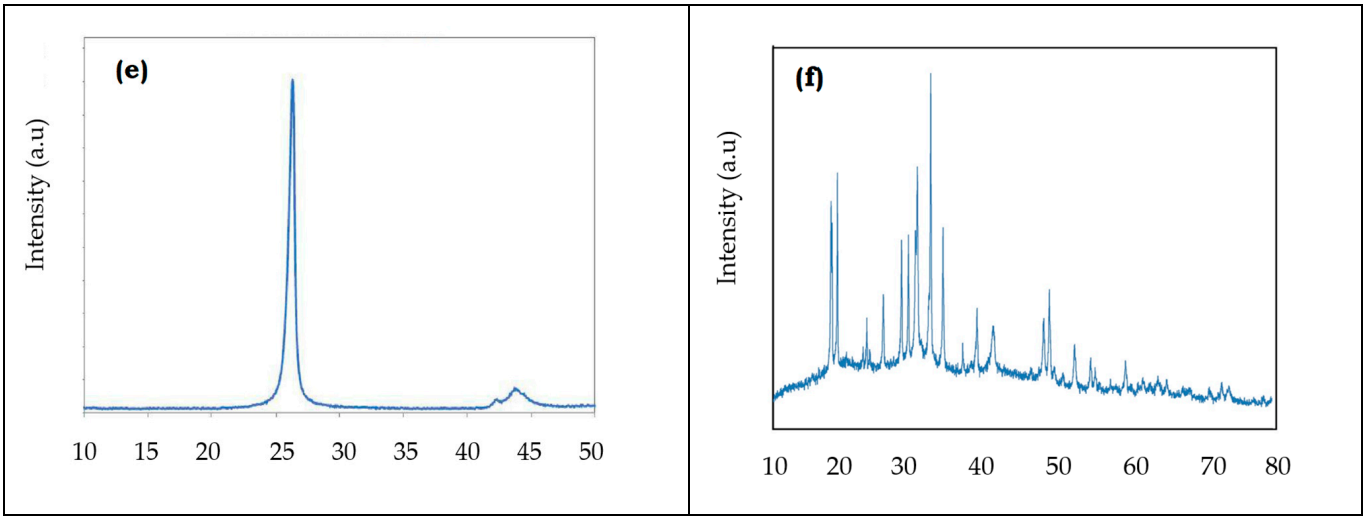


Figure 2. SEM image of (**a**) GNPs and (**b**) B_4C; EDS image of (**c**) GNPs and (**d**) B_4C; XRD image of (**e**) GNPs and (**f**) B_4C.

Table 1. Chemical composition of AZ31 alloy.

Element	Al	Zn	Mn	Si	Cu	Fe	Ni	Others	Mg
Content (%)	3.12	1.05	0.15	0.1	0.03	0.005	0.002	0.02	89.523

Table 2. Specifications of hybrid composite.

S. No	AZ31 Alloy (wt.%)	Graphene (wt.%)	Boron Carbide (wt.%)	Designation
1	98	1	1	C1
2	97	1	2	C2
3	96	1	3	C3

2.2. Experimental Procedure

Wear is the progressive diminishment of material that results from the resistance generated by friction between two surfaces. The wear test equipment (as illustrated in Figure 3) was employed to perform tribological experiments on the composite specimens in this investigation. Per the ASTM G99 standard, the specimens were manufactured with a diameter = 8 mm and a length = 30 mm. The experimentation was conducted using Taguchi's methodology. In this investigation, the output response was deemed to be the wear rate (WR), with reinforcement wt.% (R%), velocity (V), load (L), and distance (D) being the parameters with 3 levels. Levels of the parameters were determined in accordance with the material's properties and the experimental machine's capability. Table 3 contains the specifics of the factors and their respective levels that were addressed in this investigation. This study focuses on analyzing several elements and their impact on the WR. The following Expressions (1) and (2) are employed to determine the WR and COF:

$$wear\ rate\ (WR) = \frac{\triangle m}{\rho D} \quad (1)$$

$$Coefficient\ of\ Friction(COF) = \frac{\mathrm{F}}{N} \quad (2)$$

where Δm—mass loss, ρ—density (g/mm^3), D—sliding distance (m), F—frictional force (N), and N—normal force (N).

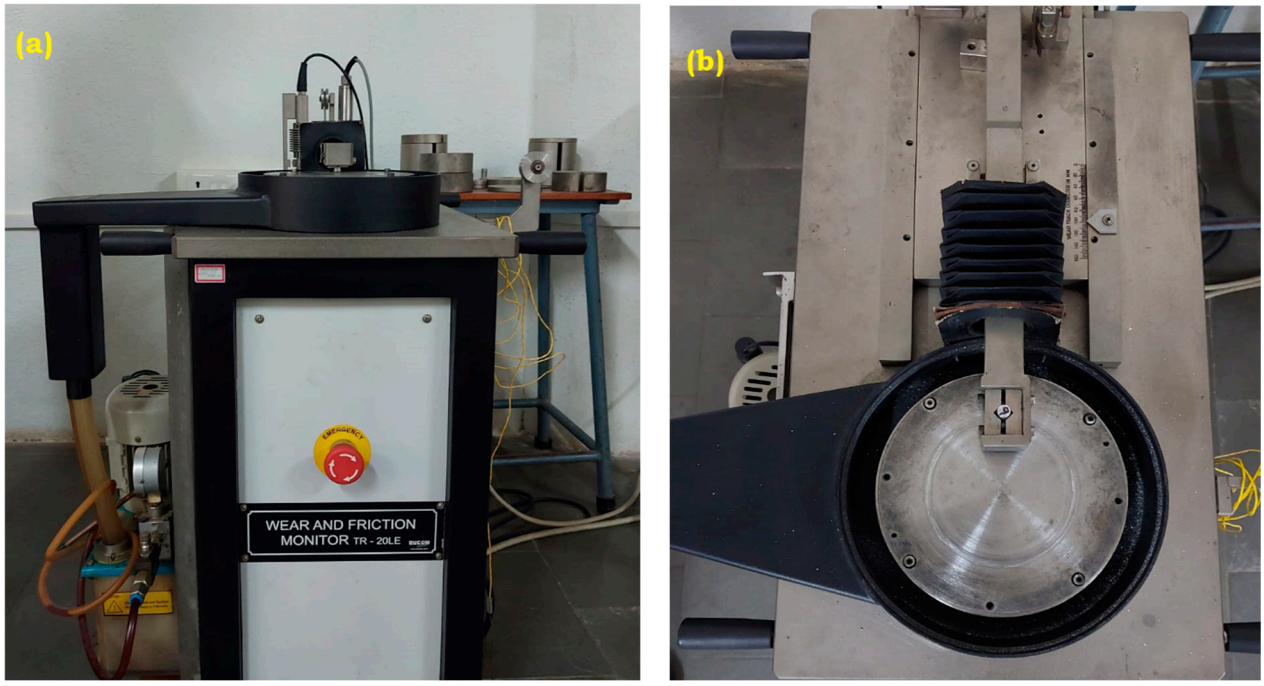


Figure 3. (**a**) Wear testing machine. (**b**) Experimental setup.

Table 3. Factors and their levels.

S. No	Factors	Level 1	Level 2	Level 3
1	Reinforcement wt.% (R %)	2	3	4
2	Velocity (V), m/s	1	2	3
3	Load (L), N	15	30	45
4	Distance (D), m	500	1000	1500

2.3. Experimental Design

The current work employed the Taguchi approach to develop the experimental runs using an L27 orthogonal array (OA). The signal-to-noise ratio (S/N) served as the primary measure in this method for ascertaining the optimal instances of the variables. The S/N ratio is a measure of the quality of a signal, calculated by dividing the intended value (mean) by the unwanted value (standard deviation). It is used to assess quality features that deviate from the desired value. Wear tests were conducted utilizing a pin-on-disk wear testing system with a track diameter of 100 mm. The tests were performed in a laboratory setting with 50–60% humidity levels and temperatures ranging from 28 to 35 °C. The tests were conducted without any lubrication, following the guidelines outlined in ASTM G99-27. The mass loss in each test was determined by comparing the initial and final weights of the specimens using electronic weighing equipment with a precision of up to 0.001 g. Figure 3 displays the experimental setup and dimensions of the specimen. Table 4 provides an extensive overview of the OA and its variables at different levels, as well as the resulting output responses.

Table 4. L_{27} OA with input parameters and output responses.

S. No	Reinforcement (R%)	Load (N)	Velocity (m/s)	Distance (m)	Wear Rate ($\times 10^{-3}$ mm^3/m)	COF (μ)
1	2	15	1	500	6.5753	0.24
2	2	15	2	1000	7.1233	0.26
3	2	15	3	1500	7.6712	0.29
4	3	30	1	500	7.1840	0.27

Table 4. *Cont.*

S. No	Reinforcement (R%)	Load (N)	Velocity (m/s)	Distance (m)	Wear Rate ($\times 10^{-3}$ mm^3/m)	COF (μ)
5	3	30	2	1000	7.8081	0.29
6	3	30	3	1500	8.1800	0.31
7	4	45	1	500	8.3825	0.28
8	4	45	2	1000	10.4147	0.29
9	4	45	3	1500	12.1928	0.21
10	3	45	1	1000	8.1800	0.29
11	3	45	2	1500	9.6672	0.36
12	3	45	3	500	6.6927	0.24
13	4	15	1	1000	4.9533	0.28
14	4	15	2	1500	5.3343	0.27
15	4	15	3	500	3.0482	0.18
16	2	30	1	1000	11.5068	0.30
17	2	30	2	1500	9.8630	0.27
18	2	30	3	500	9.4977	0.32
19	4	30	1	1500	8.6305	0.27
20	4	30	2	500	6.8584	0.28
21	4	30	3	1000	7.6205	0.21
22	2	45	1	1500	15.1307	0.35
23	2	45	2	500	10.9589	0.31
24	2	45	3	1000	13.1507	0.28
25	3	15	1	1500	5.7012	0.29
26	3	15	2	500	3.7182	0.26
27	3	15	3	1000	3.3463	0.21

3. Supervised Machine Learning (ML) Methods

In this investigation, a variety of machine learning methodologies are implemented to forecast the WR and COF of AZ31 composites. The target variables were WR and COF, while the input features were reinforcement percentage, load, velocity, and distance. Typically, the min–max scale normalizing technique is employed for normalizing experimental data in order to enhance the predictive ability of the implemented ML models. The selection of these features was determined by the literature. Regression techniques, such as polynomial, linear, and tree-based approaches, are executed through the use of Python libraries. Datasets consisting of samples of input traits and associated output responses are utilized to train the models. In order to evaluate predictive accuracy, performance assessment is carried out in conjunction with metrics such as the coefficient of determination (R^2) and the root mean square error (RMSE).

3.1. Linear Regression

Linear regression is a statistical method that is employed to investigate and quantify the relationship between two or more variables, with the specific objective of determining the impact of independent variables on a dependent variable. It is divided into two categories: simple linear regression, which involves a single independent variable, and multiple linear regression, which involves multiple independent variables. In predictive modeling, multiple linear regression is frequently implemented to predict the outcome of a dependent variable by analyzing the values of numerous predictors. The Ordinary Least Squares (OLS) method is a widely used method for estimating the parameters of a linear regression model. This method minimizes the sum of the squared differences between the predictions and observed values of the dependent variable. Effective modeling and forecasting are enabled by this method, which is particularly advantageous in time series analysis, where the relationship between variables evolves over time.

The linear regression algorithm is represented by the following expression in Equation (3):

$$Z_o = \left\{ \left(X_1^{(0)}, X_2^{(0)}, X_3^{(0)}, \ldots\ldots\ldots\ y_0 \right), \left(X_1^{(1)}, X_2^{(1)}, X_3^{(1)}, \ldots\ldots\ldots\ y_1 \right), \ldots \left(X_1^{(n)}, X_2^{(n)}, X_3^{(n)}, \ldots\ldots\ldots\ y_n \right) \right\} \quad (3)$$

The linear regression model is demonstrated in Equation (4)

$$y = c_o + \sum_{i=1}^{n} (c_i x_i) \quad (4)$$

where y—response variable, c_o —bias, x_i—independent variable (or) features c_i—coefficients or weight of x_i, and n—number of features.

3.2. Polynomial Regression

Polynomial regression is an evaluation of regression technique that includes raising each of the primary variables to a power and introducing additional variables. This is performed to assess the impact of the predictor variable x on the response variable y, using a polynomial function of degree n in x. Polynomial regression (PR) is a statistical technique that can be employed to evaluate the impact of a predictor variable x on the response variable y. The estimators for quadratic polynomial regression consist of the parameters x and x^2, while predictive variables for cubic polynomial regression consist of the parameters x, x^2, and x^3. Consequently, polynomial regression is considered a subset of multiple linear regression. This strategy provides a direct approach to examine the relationship between both dependent and independent variables

$$Z = \lambda_o + \lambda_1 y_1 + \lambda_2 y_2 + \ldots + \lambda_s y_s + \theta \quad (5)$$

where $\lambda_o,\ \lambda_1, \lambda_2, \ldots\ldots\ \lambda_n$ are known as PR coefficients, λ_o is the bias term, and $y_1, y_2, \ldots,$ y_s are denoted as independent variables,

The polynomial regression model is demonstrated in Equation (6).

$$Z = Y\lambda + \theta \quad (6)$$

where Y is the dependent variable and θ is represented as random error.

3.3. Random Forest (RF) Regression

The RF regression approach utilizes an ensemble of decision tree algorithms to predict or classify data points by combining their outcomes. This ensemble approach, which is based on trees, surpasses the constraints of conventional classification and regression tree methods. In order to reduce bias and variability, RF utilizes multiple weak decision tree learners that are generated simultaneously. The training process is gathering N bootstrapped datasets from the source database and constructing unpruned classification or regression trees from each set. In this phase, a fixed number, K, of randomly selected predictors is used instead of using all variables. This technique is repeated until T trees are produced. Combining estimations from all T trees generates up-to-date information. RF improves the diversity of trees and decreases the overall variance of the model by training trees on different subsets of data using bagging.

The expression for an *RF* regression predictor is shown below.

$$g_{RF}^{Z}(y) = \frac{1}{Z} \sum_{n=1}^{Z} DT_n(y) \quad (7)$$

where $\boldsymbol{g_{RF}^{Z}(y)}$—the aggregate prediction of the random forest model for a given input $\boldsymbol{y}$, Z—size of the ensemble, and $\boldsymbol{DT_n(y)}$—prediction from the n-th decision tree for the input y.

3.4. Gaussian Process Regression

The nonparametric Gaussian process approach is employed for significantly nonlinear problems. All input and output data are perceived as random variables, and their Gaussian distribution is automatically identified. The training dataset is utilized as input by the Gaussian process, which generates variations for all attainable functions. Therefore, the number of variables that can be applied to a Gaussian process is not restricted, and it can improve in a direct relation to the dimension of the datasets used for training. Regression employing the Gaussian process approach is characterized by the kernel function $ker(\dot{y}, \dot{y}')$ and the probability function of the mean function $n(\dot{y})$.

$$F(\dot{y}) = GP\Big(n(\dot{y}),\ ker(\dot{y}, \dot{y}')\Big) \tag{8}$$

where $\boldsymbol{n(\dot{y})}$ represents the most accurate measure of central tendency in the Gaussian model. The readings of the test input $(\dot{\boldsymbol{y}})$ are correlated to the readings of the test outcomes $(\hat{\boldsymbol{z}})$ using Equation (9).

$$\hat{z} = \mathrm{G}(y) + €\tag{9}$$

The value of € represents the variability or fluctuation of the uncorrelated variable. The effects of distinct tribological parameters on wear rate (WR) and the efficacy of each machine learning (ML) model are examined in the following section of the article.

4. Results and Discussions

The primary objective of this research is to evaluate the influence of several types of factors on the diminution of wear rate (WR). The microstructures of this research's experiments resulted in the WR and COF values, which are summarized in Table 4. Utilizing Minitab software 2021, statistical analyses were implemented. The calculated signal-to-noise (S/N) ratios for WR were used to generate a response table for the S/N values of WR. This table offers a comprehensive understanding of the efficacy of each factor on the WR. In Table 5, the response table employs a ranking system to denote the impact of each factor on the outcome. An extremely influential factor is represented by rank 1, while a factor with minimal influence is represented by rank 4.

Table 5. Density and hardness of the AZ31 hybrid composites.

Composite	Density (g/cm^3)	Hardness (HB)
C1	1.78 ± 0.005	68 ± 2
C2	1.82 ± 0.011	76 ± 3
C3	1.86 ± 0.016	87 ± 5

4.1. Microstructure Analysis

The composite specimens are illustrated in SEM images in Figure 4. It indicates the existence of a vital α-Mg matrix, which is surrounded by a distributed α eutectic phase. Furthermore, remnants of β eutectic are identified within the distributed α eutectic zone. The eutectic phases were uniformly distributed along the grain's peripheral borders. The Al-enriched fraction of the liquid metal underwent a separated eutectic reaction, which resulted in the formation of these phases. While the majority of the α-phases were positioned in close alignment to the eutectic phases, only a handful of α-phases were dispersed within α-Mg crystals. The eutectic phases at the boundaries of the grains of the composite are likely to produce a lamellar microstructure. The incorporation of B_4C and Gr into the matrix transformed the lamellar eutectics into completely dissociated β eutectics, as illustrated in Figure 4. Precipitates were also found at the interfaces between individual grains. The specimens exhibit remarkable grain and grain border visibility. The SEM scans indicate that all specimens have a highly dense microstructure. Moreover, the microstructure had no pore characteristics. The reinforced specimens include a homogeneous distribution of B_4C

and graphene particles throughout the grain boundaries. The mechanical properties, such as density and hardness, are depicted in Table 5. The Brinell hardness test was conducted on polished AZ31 composites to assess their hardness values, utilizing an indentation load of 250 kgf for a duration of 15 s, in accordance with ASTM E10-18. Each reading comprised at least three separate measurements taken from random spots on the specimens' surface. From the outcomes, it is observed that the density and hardness of the composites increased with the increase in the wt.% of reinforcements. Further, improvement in hardness can be attributed to heterogeneous nucleation and grain refinement, which result from the presence of minute nanoparticles.

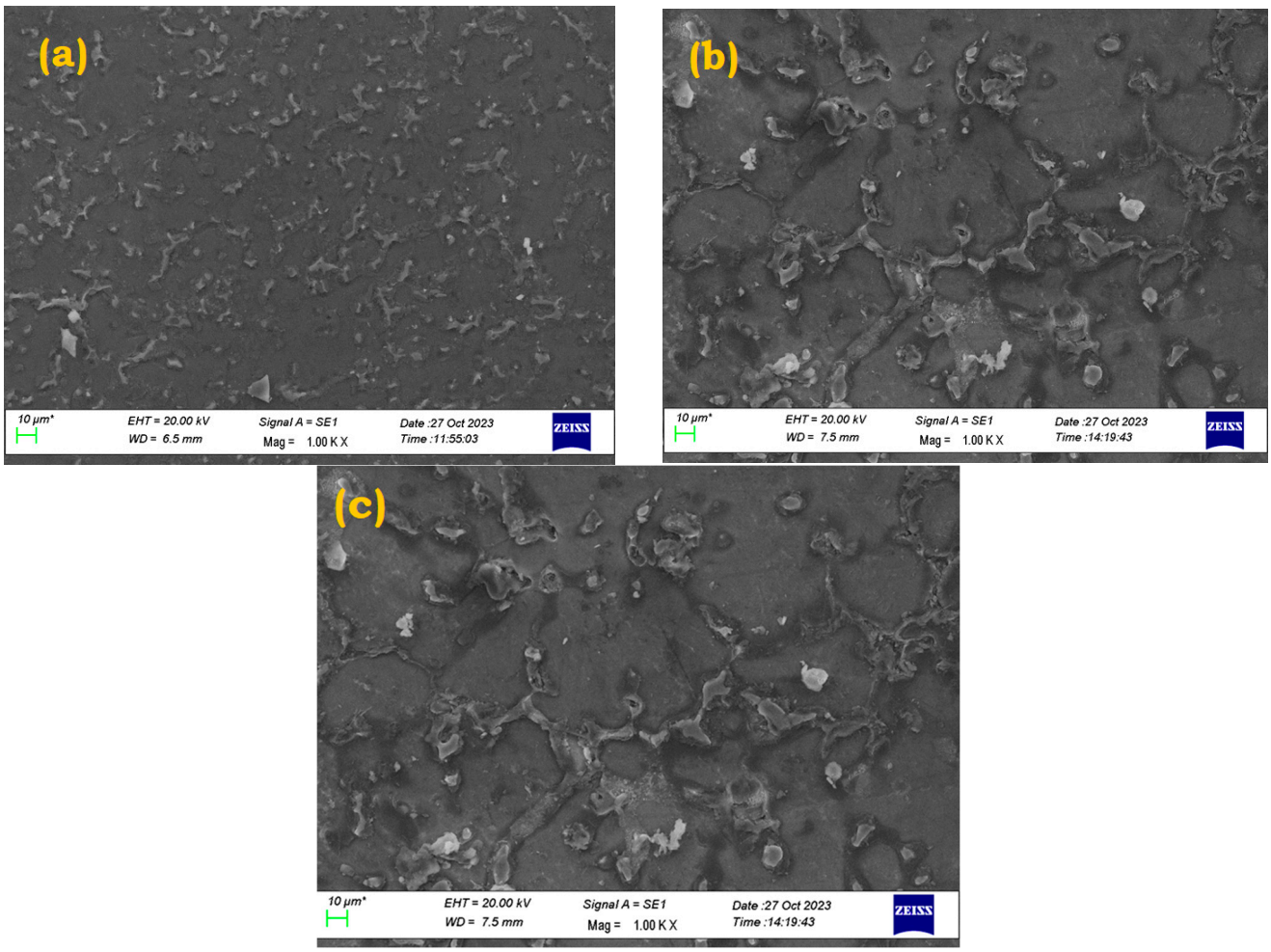


Figure 4. SEM microstructures of (**a**) AZ31 + 1 wt.% graphene + 1 wt.% B_4C; (**b**) AZ31 + 1 wt.% graphene + 2 wt.% B_4C; and (**c**) AZ31 + 1 wt.% graphene + 3 wt.% B_4C.

4.2. Taguchi Analysis

The key objective of this investigation is to reduce the wear rate (WR). Consequently, the signal-to-noise (S/N) ratio was determined by employing the "smaller is better" criterion. Table 6 displays the S/N ratio responses for the WR data, with the load (L) accounting for the maximum delta value, indicating that it is the most significant factor. Consequently, it was discerned that load (L) had the most significant impact on WR, with D, R%, and V following in that order. To differentiate between input factors that were significant and those that were insignificant in relation to the output responses, ANOVA was implemented. The results of the ANOVA were determined with a 95% confidence level (p = 0.05), which suggests that variables with a P-value less than 0.05 have a significant impact on the outcome. Furthermore, Table 7 supports this assertion by verifying that load (L) is the primary factor contributing to WR, accounting for 55.87% of the variation.

Table 6. Response table for signal to noise ratios.

Level	R%	L	V	D
1	−16.93	−10.80	−15.22	−12.46
2	−14.68	−15.98	−14.94	−15.35
3	−13.08	−17.90	−14.53	−16.88
Delta	3.85	7.10	0.69	4.42
Rank	3	1	4	2

Table 7. Analysis of variance for means.

Source	DF	Seq SS	Adj SS	Adj MS	F	P	Contribution %
R%	2	27.185	27.185	13.5926	35.26	0.000	17.34
L	2	87.605	87.605	43.8027	113.63	0.000	55.87
V	2	0.605	0.605	0.3025	0.78	0.498	0.39
D	2	34.798	34.798	17.3990	45.14	0.000	22.19
L × V	4	0.193	0.193	0.0483	0.13	0.968	0.12
L × D	4	2.167	2.167	0.5417	1.41	0.337	1.38
V × D	4	1.932	1.932	0.4829	1.25	0.383	1.23
Residual Error	6	2.313	2.313	0.3855			1.48
Total	26	156.798					100

As the load is increased, it is evident that WR increases, as illustrated in Figure 5. The composite material that contained a higher level of reinforcement, such as C3, demonstrated greater resistance to wear when compared with various composites. The composite's enhanced strength and hardness can be the result of the enhanced reinforcement. At increasing loads, the wear rate (WR) increases due to enhanced friction between the pin and disk, resulting in the loss of material from the pin. Furthermore, it has been noted that the composites demonstrate enhanced wear resistance in comparison to the alloy under consistent sliding velocity and load contexts [18]. When the load is reduced, it is expected that there will be a decrease in the interaction between the mating surfaces. This little contact may lead to a decrease in the water resistance of the processed samples. On the other hand, when there were more loads, the interaction between the surfaces that were in touch improved. As a result, this caused a rise in WR and a decrease in the surface's wear resistance [19]. During the wear studies, the presence of embedded particles led to a decrease in the impact of the applied load. The presence of embedded particles serves as a barrier, which decreases the effects of plastic deformation and results in a significant improvement in wear resistance [20]. Subsequently, the sliding distance was identified as the second most influential factor affecting wear rate. The WR increases as the sliding distance extends, as indicated by the observations in Figure 5. When the applied load attained its maximum value, the sliding distance's impact became more pronounced. This behavior is associated with the thermal energy that is produced between the two mating surfaces during abrasive wear. The test material was softened as a result of the increased heat generated as the sliding distance increased. The bonding strength between the matrix material and the reinforced particles was diminished as a result of this softening, which increased the likelihood of particle detachment during abrasion. Furthermore, the instability of the tribo-layer at longer sliding distances may also contribute to this effect. The next influential factor on the WR is reinforcement percentage (R%). It is widely recognized that the matrix's resilience is significantly influenced by the reinforcement within it. As the adhesion between the matrix and the reinforcing material increases, the matrix material's rigidity and resistance are also improved. Reinforcement materials are incorporated into the composite material, which results in an increase in its hardness. It is possible to reduce the rate of wear by increasing the hardness of the composite material, which in turn contributes to its improved wear resistance. Similarly, there is a commensurate reduction in contact time as the velocity increases, which leads to a decrease in WR. Increasing velocity results in an upsurge in heat generation over the disk and pin due to the friction across

the surfaces that slide. At elevated temperatures, the Mg on the pin endures substantial plastic deformation, which leads to the formation of an oxide surface. Smooth gliding of the mating surface is facilitated by the application of this surface mixture, resulting in a decrease in the WR. The existing research [12] has shown a similar tendency with load and velocity. Figure 6. illustrates the main effects plot of S/N ratios for WR data. The factor levels at which optimization has occurred are explicitly identified in this plot. The parameters that are ideal for alleviating WR are R% = 4, L = 15 N, V = 3 m/s, and D = 500 m, as illustrated in Figure 6.

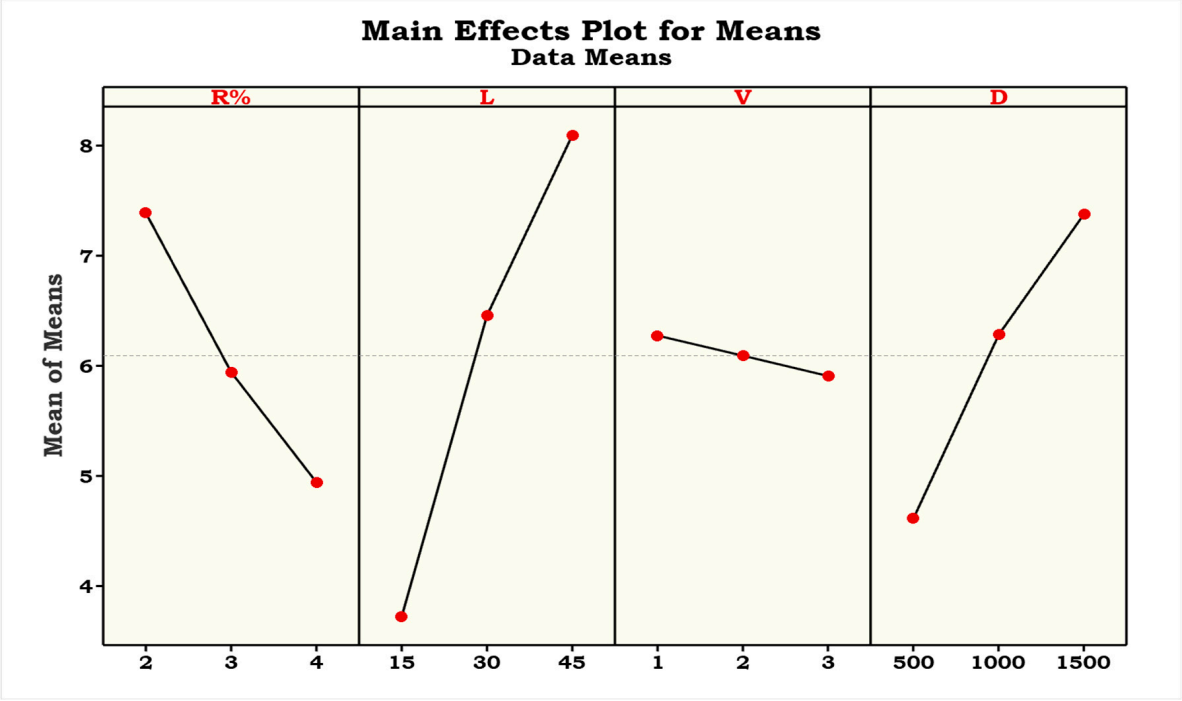


Figure 5. Effect of various factors on WR (means data).

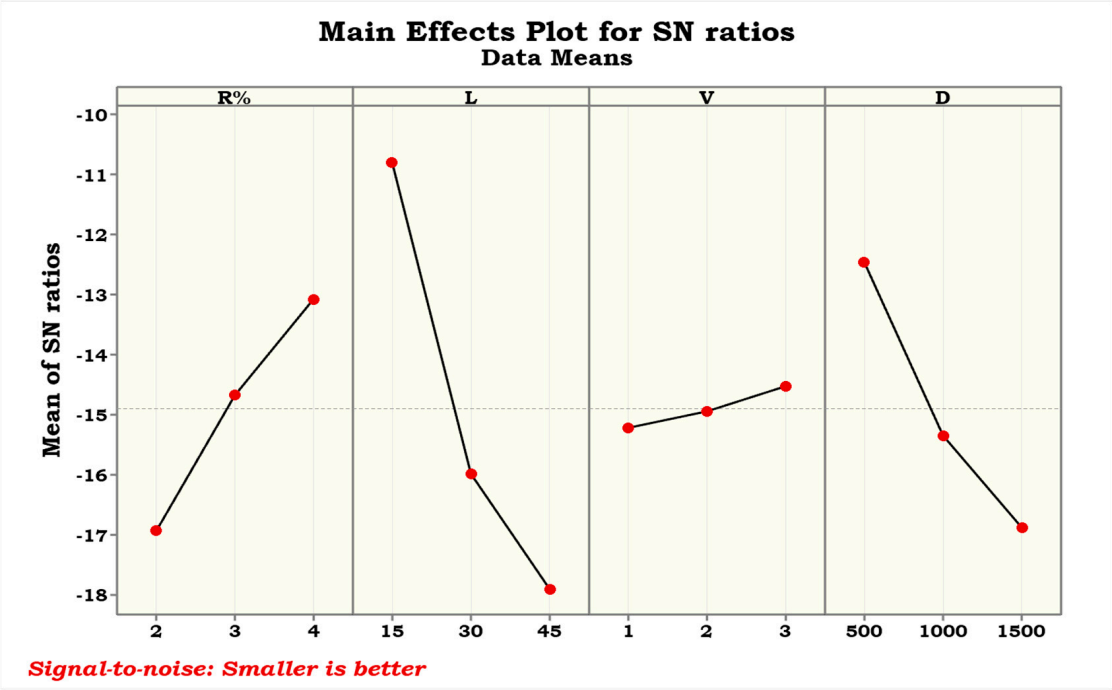


Figure 6. Effect of various factors on WR (S/N ratios data).

The interaction plot for means as shown in Figure 7 illustrates the interaction effects between the factors L (load), V (velocity), and D (distance) on the response variable, likely the wear rate (WR) or a related metric. From the load vs. velocity plot, it is observed that as the load (L) increases from 15 to 45 N, the response variable generally increases across all levels of velocity (V). The effect of velocity is more pronounced at higher loads. For example, at L = 45, the increase in response is steeper as V increases. From the load vs. distance plot, similar to the L vs. V interaction, the response variable increases with increasing load across all distances. The impact of distance (D) on the response seems consistent, with the response increasing steadily as D increases, especially noticeable at the highest load (L = 45). As per the velocity vs. distance graph, it can be understood that as velocity (V) increases, the response variable also increases across all distances. The effect of distance on the response is somewhat consistent across different velocities, with higher distances leading to higher response values. The parallel lines in the L vs. V and L vs. D plots suggest that there is minimal interaction between these factors. This means that the effect of one factor on the response is relatively independent of the other. The V vs. D plot shows slight convergence and divergence in lines, indicating some interaction between velocity and distance, but the effect is not very strong. Load (L) appears to have the most significant effect on the response, with the highest response values seen at the highest load (L = 45) across all other factors. Velocity (V) and distance (D) also influence the response, but their effects are secondary to load. The increase in the response variable with higher V and D is more evident at higher loads. This plot helps identify how the combination of different factor levels impacts the response, which can guide optimization efforts.

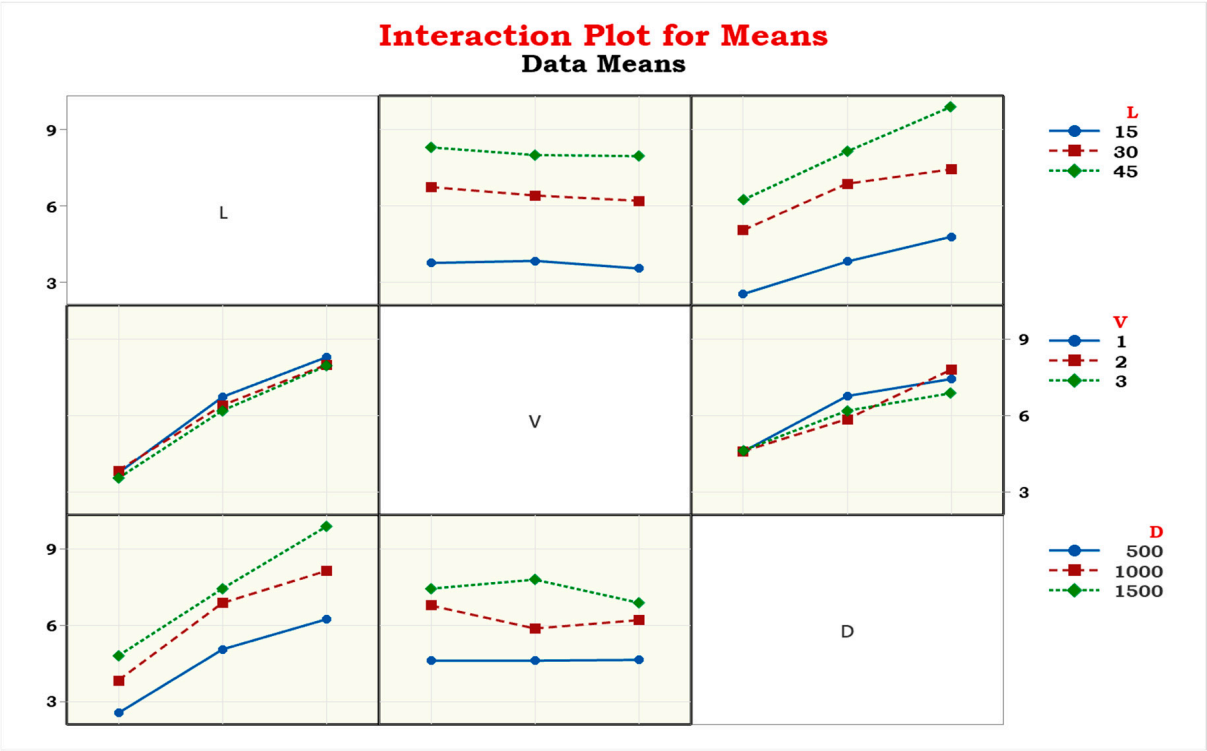


Figure 7. Interaction plot for means.

In order to evaluate the residuals of a statistical model that is associated with the means, the graph in Figure 8 comprises four residual plots. The Normal Probability Plot evaluates the likelihood of residuals being normal. It is desirable for the residuals to be located along the diagonal. Although there are some deviations at the extremes, the residuals are approximately normally distributed, as evidenced by the fact that the majority of points in this plot lie along the line. The residuals versus fits plot displays the residuals in comparison to the fitted values. The objective is to identify any patterns that may

suggest problems with the model's fit, such as heteroscedasticity (change in variance) or nonlinearity. The residuals are random and lack a discernible pattern, which implies that the model does not exhibit any apparent issues with nonlinearity or unequal variance. The residuals are represented by the histogram, which illustrates their frequency distribution. Around zero, the distribution appears to be somewhat symmetrical, albeit with a degree of skewness. According to the general bell shape, the residuals may adhere to a normal distribution, albeit with a slight deviation. The versus order plot displays residuals in the order of data collection to identify any patterns that may suggest a correlation between errors that may appear over time. This indicates that the residuals are not significantly affected by autocorrelation or time-related bias, as they fluctuate arbitrarily around zero.

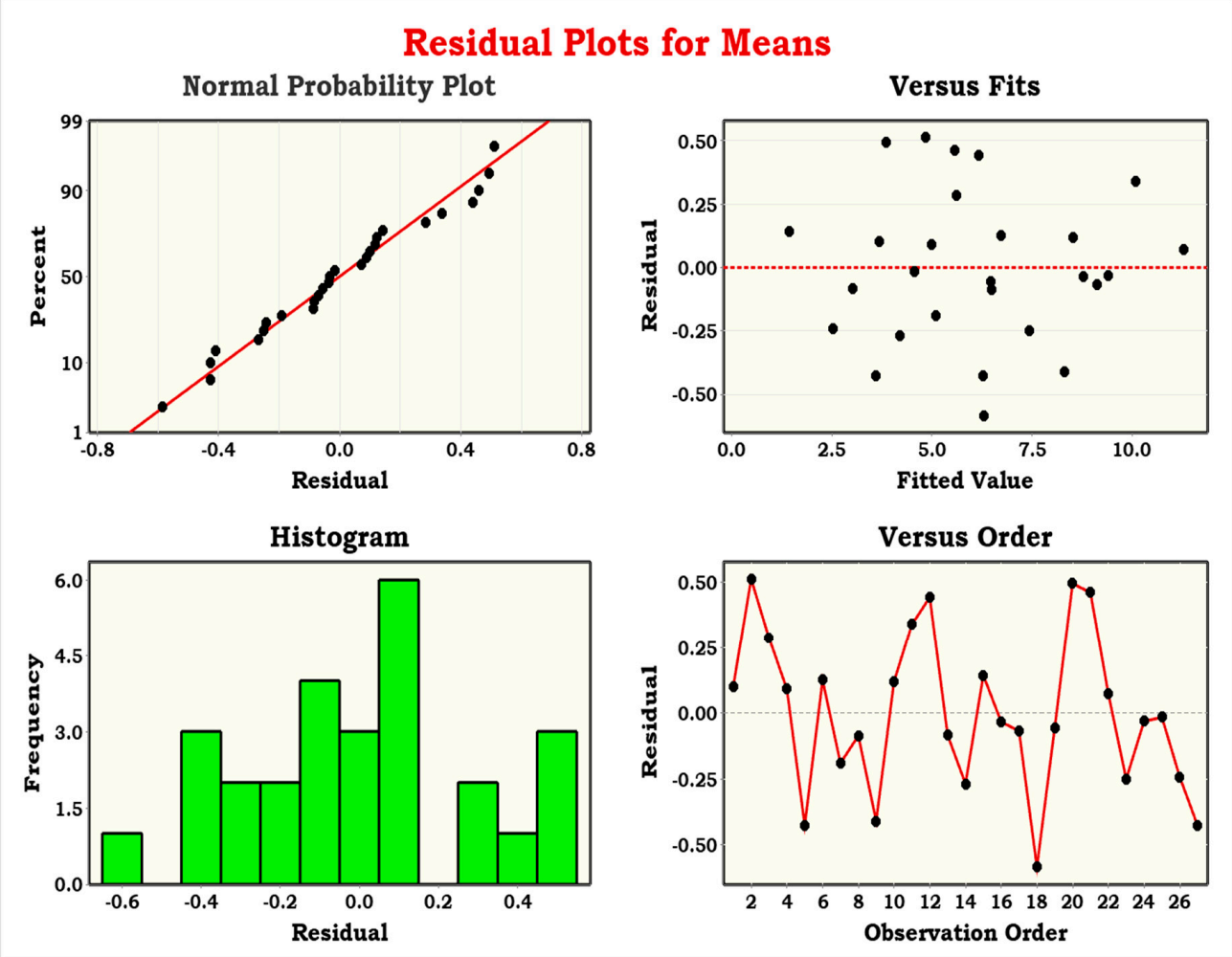


Figure 8. Residual plots for WR.

4.3. Wear Surface Analysis

Figure 9 displays scanning electron microscope (SEM) images that illustrate the surface morphology of the hybrid composites' most and least worn-out surfaces. Composite C1 exhibited the maximum wear rate in the experimental results when subjected to a load (L) of 45 N, a sliding velocity (V) of 1 m/s, and a distance (D) of 1500 m. Conversely, the composite C3 exhibited the lowest attrition rate at L = 15 N, V = 3 m/s, and D = 500 m. Composites are generally subjected to a diverse array of wear mechanisms, such as oxidation, delamination, adhesion, and attrition [18,21]. SEM micrographs of the high-wear pin surface were illustrated in Figure 9a,b. From the figure, it was discerned that the surface contains plowing areas and broader grooves. It was noted that the grooves' width and depth were enhanced under high attrition conditions, with a load of 45 N. The abrasion mechanism is dominated by the

load, as evidenced by this. Based on the observations from Figure 9a,b, it can be concluded that the surface exhibits a rough and uneven texture, indicating substantial wear of the material. The presence of roughness suggests the process of removing material or causing abrasion. There appear to be minute fissures or fractures on the surface. These are most likely caused by mechanical stress that occurs throughout the process of wearing. Cracks in the composite material can undermine its strength, resulting in increased deterioration and the risk of failure. There is a build-up of trash or small particles on the surface. This may be attributed to the erosion of the substance during the procedure. These particles have the potential to impact the friction and wear properties of the composite material. There are regions on the surface that appear as depressions or empty spaces. Pitting may occur as a consequence of localized material erosion, may be caused by mechanical fatigue or the degradation of certain phases within the hybrid composite. The scans (Figure 9a,b) exhibit differences in the surface, implying that different materials within the composite are experiencing distinct rates of wear. This phenomenon is frequently observed in hybrid composites, where various phases or components may exhibit disparate levels of hardness or resistance to wear. The scanning electron microscope (SEM) pictures (Figure 9a,b) demonstrate that the hybrid composite has seen substantial wear, resulting in a rough, fragmented, and pockmarked surface. The existence of fissures, debris, and surface heterogeneity suggests that the material has experienced significant mechanical strain resulting in deterioration. This type of surface morphology is commonly found in situations where the composite material is subjected to significant amounts of friction, stress, or abrasive pressures. The SEM images of the low-worn surface, as depicted in Figure 9c,d, exhibited parallel grooves that are presumably the result of sliding wear. Although these grooves are relatively shallow, they are indicative of low wear conditions, as they indicate minimal material elimination. Scattered detritus and small particles are visible in the grooves. This could be the result of minor abrasive action or wear particulates that have not been completely removed from the surface. It appears that the surface is largely unaltered, with only a few significant scratches or pits. The material's ability to maintain its integrity under the applied load, velocity, and distance is indicated by the absence of substantial surface damage, which is indicative of a low attrition rate. In this instance, the absence of substantial wear traces or extensive pitting indicates that abrasive wear is the primary mechanism, with minimal contributions from adhesion or delamination. This is consistent with a lower wear rate, as the wear particles appear to be thin and well-dispersed. In conclusion, this hybrid composite surface that has undergone low wear is characterized by shallow grooves, minimal surface damage, and the presence of fine detritus, which suggests a relatively mild wear process.

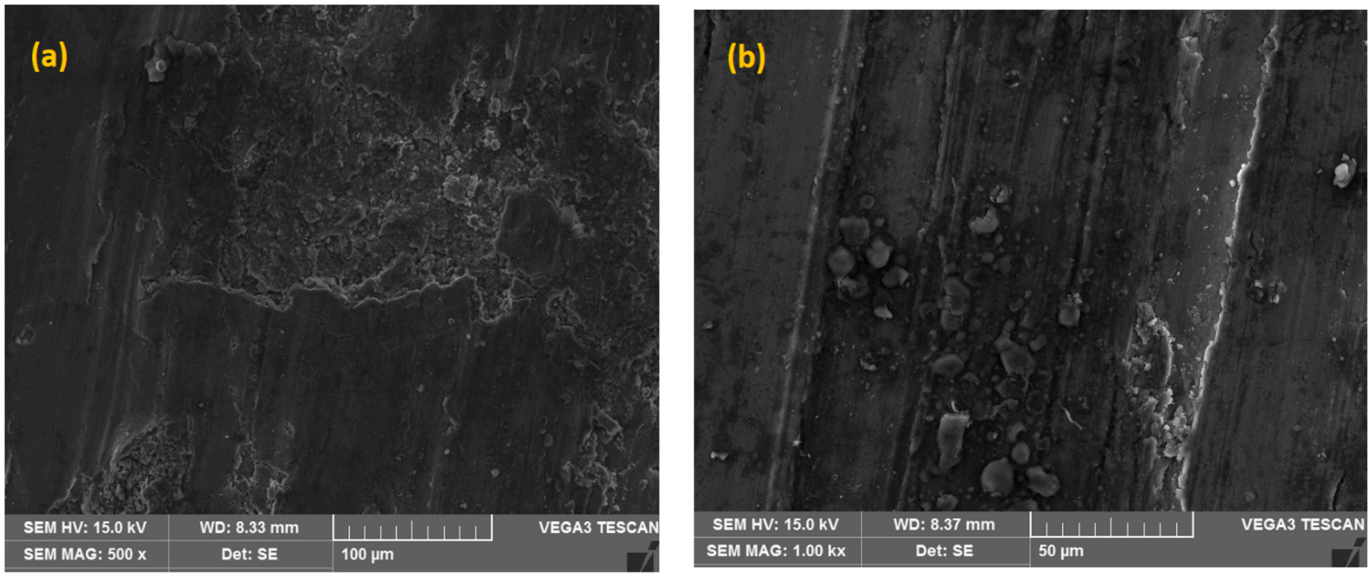


Figure 9. *Cont.*

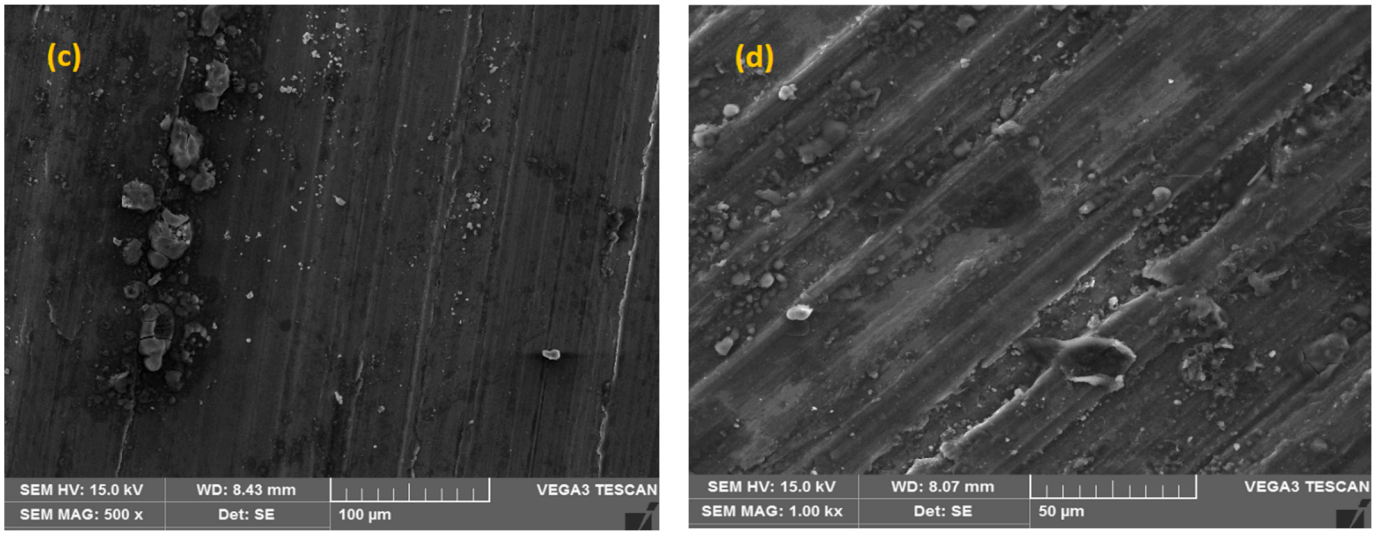


Figure 9. (**a**,**b**) High worn surfaces. (**c**,**d**) Low worn out surfaces.

5. Performance Evaluation of ML Techniques

The assessment of the accuracy and variability of a machine learning model implemented to predict the wear properties of AZ31 hybrid composites was investigated using statistical measures [22]. In the current work, to evaluate the performance of ML techniques, 24 data points (90% of the data) are used for training, and the remaining 3 points (10% of the data) are employed for testing. The present study employs the coefficient of determination (R^2), mean squared error (*MSE*), and root mean squared error (*RMSE*) as assessment metrics for the test dataset of WR, which consists of 3 experimental data points. These metrics provide a numerical evaluation of how well a machine learning model accurately reflects the real experimental data (Equation (10)—[23] and Equation (12)—[24]).

$$MSE = \frac{1}{m}\sum_{i=1}^{m}\left(z_p - z_a\right)^2 \tag{10}$$

$$RMSE = \sqrt{MSE} \tag{11}$$

$$R^2 = 1 - \frac{\sum_{i=1}^{m}\left(z_p - z_a\right)^2}{\sum_{i=1}^{k}\left(z_p - \overline{z}_a\right)^2} \tag{12}$$

where z_a and z_p depict the actual and predicted values of the outcomes.

In order to exhibit the precision of the machine learning models that are generated, a scatter plot is typically implemented. A substantial quantity of variation exists between the experimental results and the predicted results obtained by various machine learning models, as illustrated in Figures 10 and 11. Red line represents the reference line and circle depicts the data value in the provided Figure. The expected wear rate and COF data are displayed alongside a regression diagonal line connecting the actual and predicted results. It is essential to observe that all the dispersed projected values should approximate the diagonal line to attain enhanced accuracy. A robust model is indicated by a high R^2 value when the scatter points are closely clustered around the diagonal line [25]. It was observed that the scattered dispersion of the PR machine learning models is more concentrated along the center line than that of the LR, RF, and GPR models (refer to Figures 10 and 11). The PR model shows the lowest variance (around the diagonal line) and the finest scatter dispersion of points across all models. Figures 10e and 11e illustrate a comparison of the experimental and predicted wear rate (WR) and coefficient of friction (COF) for the various models examined in this work. An analysis of this graphic indicates that, among all machine learning models, the anticipated results of the trained and examined datasets of the PR model closely aligned with the results of the experiments.

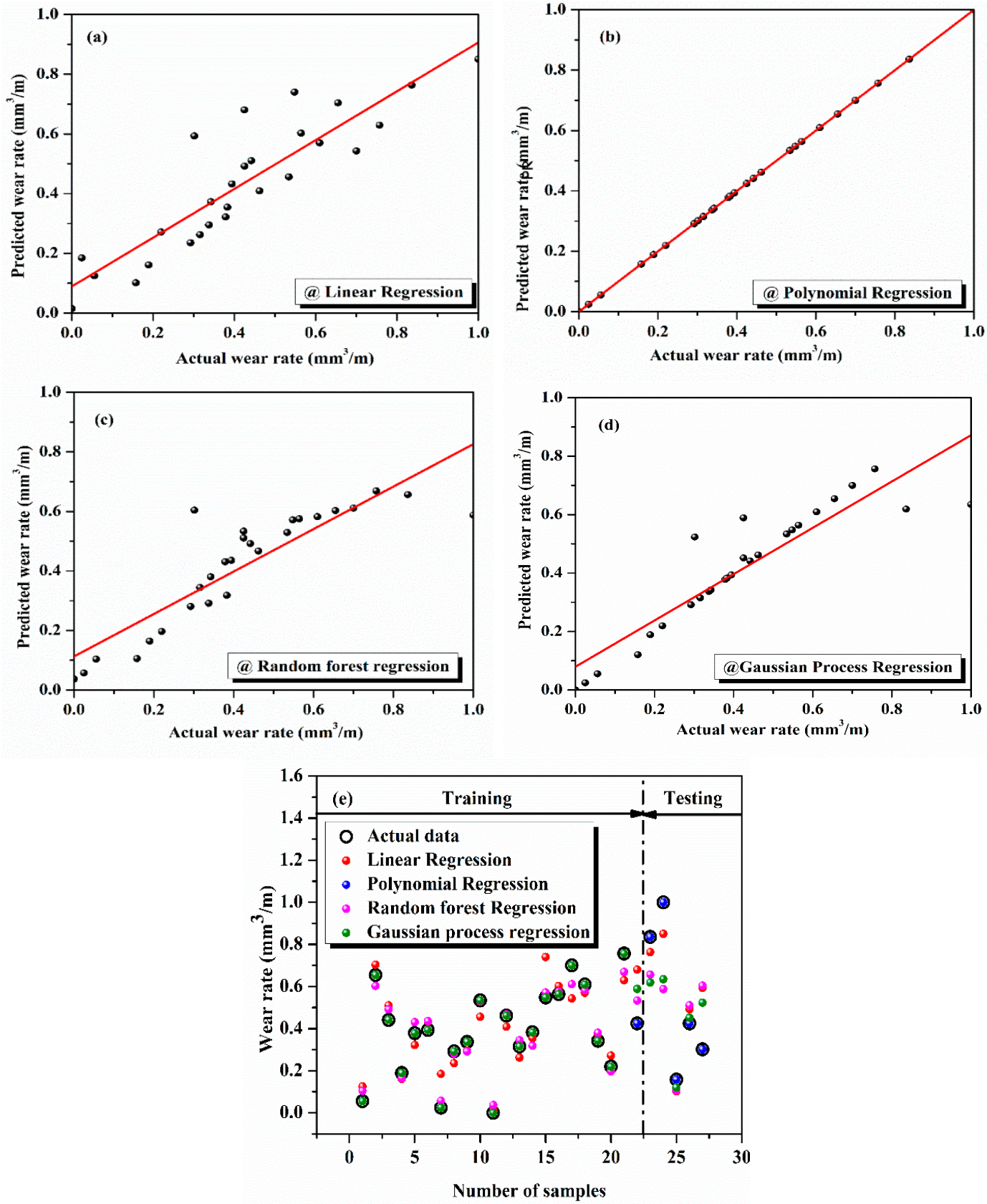


Figure 10. Regression plots for WR data with (**a**) LR, (**b**) PR, (**c**) RF, and (**d**) GPR. (**e**) Comparison plot for training and testing of LR, PR, RF, and GPR techniques.

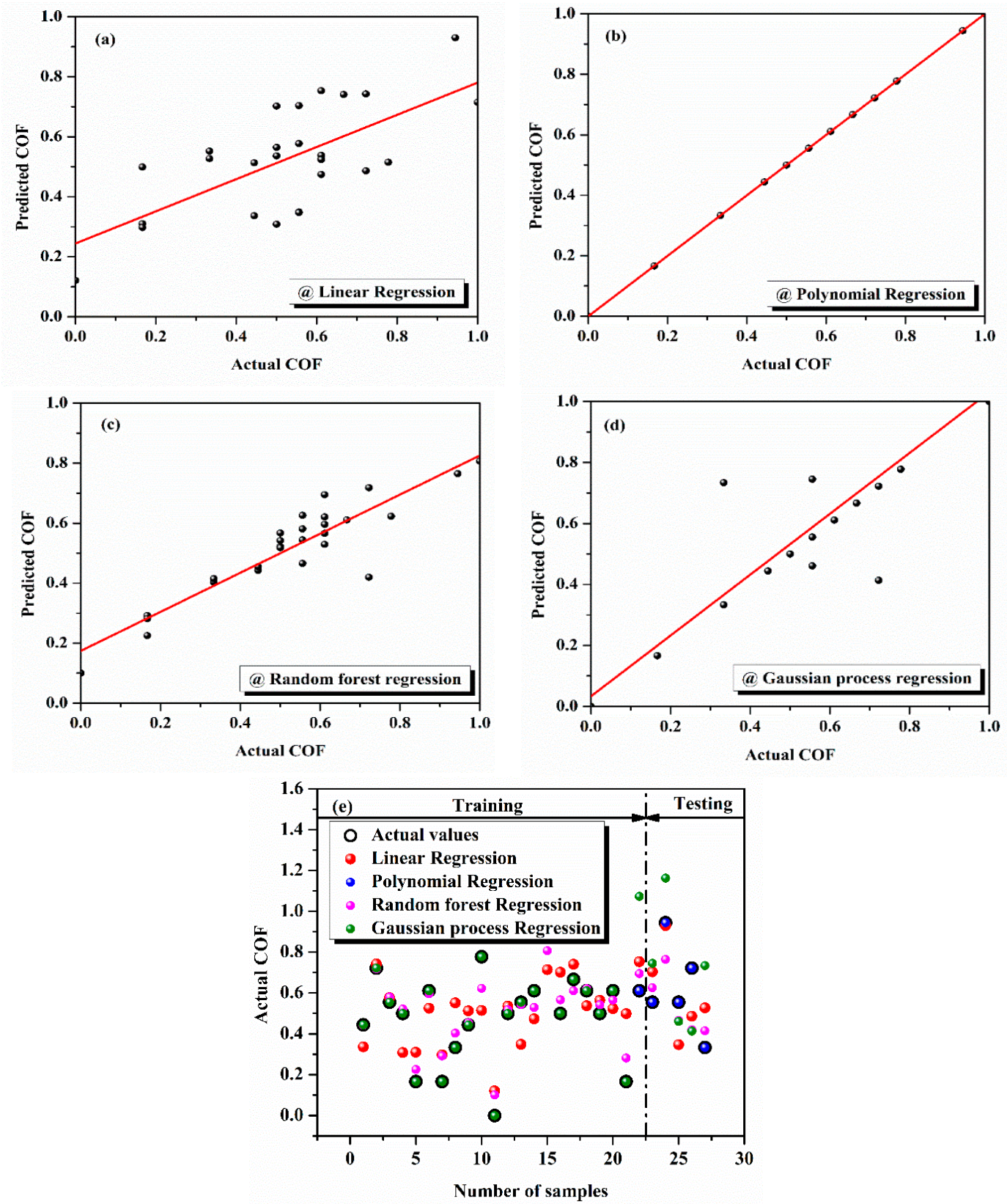


Figure 11. Regression plots for COF data with (**a**) LR, (**b**) PR, (**c**) RF, and (**d**) GPR. (**e**) Comparison plot for training and testing of LR, PR, RF, and GPR techniques.

The statistical measures of the machine learning (ML) models for the wear rate (WR) and COF of the test data are presented in Table 8. The accuracy of the WR and COF

predictions produced by the models ranges from 0.207 to 0.953 and 0.272 to 0.937. In addition, the MSE, RMSE, and MAE values are remarkably low. The metrics utilized in this study indicate that the derived models display a good level of precision in estimating the WR (wear rate) of AZ31 MMCs using the provided input parameters. Table 8 demonstrates a noticeable enhancement in accuracy, as evidenced by the R^2 values, while moving from LR to GPR. This is then followed by a decrease in other error metrics. In accordance with statistical specifications, the PR model demonstrated a high level of accuracy in its predictions for WR (0.953) and COF (0.937).

Table 8. Performance analysis of various ML models for the test datapoints.

Data	ML Model	MSE	RMSE	R^2
WR	LR	0.056	0.236	0.647
	PR	0.011	0.103	0.953
	RF	0.041	0.201	0.689
	GPR	0.017	0.129	0.807
COF	LR	0.021	0.176	0.532
	PR	0.031	0.114	0.937
	RF	0.025	0.158	0.648
	GPR	0.016	0.126	0.772

6. Conclusions

In this study, the influence of various wear parameters, including reinforcement percentage (R%), velocity (V), load (L), and distance (D), on the wear rate (WR) of magnesium composites was effectively examined. In order to optimize the design of the experiments and analysis, the Taguchi method was implemented. Numerous machine learning algorithm models were generated in order to identify the most efficient prediction method using the most optimal parameters. The main findings derived from the current investigation are as follows:

- The findings indicate that the load is the most critical variable affecting WR, followed by distance (D), reinforcement (R%), and velocity (V).
- Based on the mean effect illustrations for WR, the ideal conditions for achieving the lowest WR are R% = 4, L = 15 N, V = 3 m/s, and D = 500 m.
- The wear resistance of the AZ31 composite with a higher concentration of B_4C demonstrates superior wear resistance attributable to its elevated hardness compared to other materials.
- Wear rate was diminished for low load, short distance, and high velocity, whereas it peaked at high load, extended distance, and low velocity.
- The wear mechanisms of oxidation, delamination, and abrasion are discernible in both minimal and extreme wear conditions. The findings of the SEM investigation show that abrasion and delamination are frequently encountered under higher wear conditions, whereas abrasion is more prevalent under low wear surfaces.
- Analysis of the regression and comparative graphs revealed that the PR model has superior predictive capacity for the tested data of WR (R^2 = 0.953, MSE = 0.011, and RMSE = 0.103) and COF (R^2 = 0.937, MSE = 0.013, and RMSE = 0.114).

Author Contributions: Conceptualization, D.K.A., B.K.C., B.G., R.K.K., R.A., T.S.R., S.P. and R.K.; methodology, D.K.A., B.K.C., B.G., R.K.K., R.A., T.S.R., S.P. and R.K.; software, D.K.A., B.K.C., B.G., R.K.K., T.S.R., S.P. and R.K.; validation, D.K.A., B.K.C., B.G., R.K.K., T.S.R., S.P. and R.K.; formal analysis, D.K.A., B.K.C., B.G., R.K.K., T.S.R., S.P. and R.K.; investigation, D.K.A., B.K.C., B.G., R.K.K., T.S.R., S.P. and R.K.; resources, D.K.A., B.K.C., B.G., R.K.K., T.S.R., S.P. and R.K.; data curation, D.K.A., B.K.C., B.G., R.K.K., T.S.R., S.P. and R.K.; writing—original draft preparation, D.K.A., B.K.C., B.G., R.K.K., R.A., T.S.R., S.P. and R.K.; writing—review and editing, R.K.K., R.A. and S.P.; visualization, D.K.A., B.K.C., B.G., R.K.K., T.S.R., S.P. and R.K.; supervision, R.K.K., S.P. and R.K.;

project administration, R.K.K., S.P. and R.K.; funding acquisition, S.P. and R.K. All authors have read and agreed to the published version of the manuscript.

Funding: Support from the Ministry of Science and Higher Education of the Russian Federation (Ural Federal University Program of Development within the Priority-2030 Program) is gratefully acknowledged: grant Number FEUZ-2022-0031.

Data Availability Statement: Data is contained within the article.

Acknowledgments: Aepuru acknowledge the project Competition for Research Regular Projects, year 2021, code LPR21-03, Universidad Tecnológica Metropolitana (UTEM). Aepuru acknowledges Department of Mechanical Engineering, Universidad de Chile.

Conflicts of Interest: The authors declare that they have no known competing financial interests or personal relationships that could have appeared to influence the work reported in this paper.

References

1. Kulekci, M.K. Magnesium and Its Alloys Applications in Automotive Industry. *Int. J. Adv. Manuf. Technol.* **2008**, *39*, 851–865. [CrossRef]
2. Gupta, M.; Sharon, N.M.L. *Magnesium, Magnesium Alloys, and Magnesium Composites*, 1st ed.; John Wiley & Sons, Inc.: Hoboken, NJ, USA, 2011; ISBN 9780470494172.
3. Tan, J.; Ramakrishna, S. Applications of Magnesium and Its Alloys: A Review. *Appl. Sci.* **2021**, *11*, 6861. [CrossRef]
4. Ammisetti, D.K.; Sai Sarath, K.; Kruthiventi, S.S. A Review on Mechanical and Wear Characteristics of Magnesium Metal Matrix Composites. *J. Tribol.* **2024**, *147*, 020801. [CrossRef]
5. Wang, H.Y.; Jiang, Q.C.; Wang, Y.; Ma, B.X.; Zhao, F. Fabrication of TiB_2 Participate Reinforced Magnesium Matrix Composites by Powder Metallurgy. *Mater. Lett.* **2004**, *58*, 3509–3513. [CrossRef]
6. Khatkar, S.K.; Verma, R.; Kant, S.; Suri, N.M. Optimization of Wear Behavior of AZ91D-SiC-Gr Hybrid Composites Using Taguchi Experimental Design. *Adv. Intell. Syst. Comput.* **2020**, *1053*, 1151–1163. [CrossRef]
7. Tajdeen, A.; Megalingam, A.; Sivanesh Prabhu, M.; Wasim Khan, M. Role of Tungsten Disulfide Particles on the Microstructure, Mechanical, and Tribological Behaviors of Friction Stir-Processed Magnesium-Based Composite. *J. Tribol.* **2023**, *145*, 014501. [CrossRef]
8. Vedabouriswaran, G.; Aravindan, S. Wear Characteristics of Friction Stir Processed Magnesium RZ 5 Composites. *ASME J. Tribol.* **2019**, *141*, 041601. [CrossRef]
9. Li, C.D.; Wang, X.J.; Wu, K.; Liu, W.Q.; Xiang, S.L.; Ding, C.; Hu, X.S.; Zheng, M.Y. Distribution and Integrity of Carbon Nanotubes in Carbon Nanotube/Magnesium Composites. *J. Alloys Compd.* **2014**, *612*, 330–336. [CrossRef]
10. Sari, F.N.; Karamis, M.B.; Kaya, Y. Friction Characteristics of Hybrid Magnesium Alloy Composites Reinforced with Carbon Nanotube and Cerium. *Ind. Lubr. Tribol.* **2017**, *69*, 52–58. [CrossRef]
11. Kaviti, R.V.P.; Jeyasimman, D.; Parande, G.; Gupta, M.; Narayanasamy, R.; Koppad, P.G. Improving the Friction and Wear Characteristics of AZ31 Alloy with the Addition of Al_2O_3 Nanoparticles. *Mater. Res. Express* **2019**, *6*, 126505. [CrossRef]
12. Kartheesan, S.; Shahul Hamid Khan, B.; Kamaraj, M.; Tekumalla, S.; Gupta, M. Dry Sliding Wear Behavior of Magnesium Nanocomposites Using Response Surface Methodology. *J. Tribol.* **2022**, *144*, 011704. [CrossRef]
13. Abebe, S.K.; Beri, H.; Sinha, D.K.; Rajhi, A.A.; Hossain, N.; Duhduh, A.A.; Zainuddin, S.; Mohammed, G.; Ahmed, S. Wear Behavior of AZ61 Matrix Hybrid Composite Fabricated via Friction Stir Consolidation: A Combined RSM Box—Behnken and Genetic Algorithm Optimization. *J. Compos. Sci.* **2023**, *7*, 275. [CrossRef]
14. Jalilvand, M.M.; Mazaheri, Y. Effect of Mono and Hybrid Ceramic Reinforcement Particles on the Tribological Behavior of the AZ31 Matrix Surface Composites Developed by Friction Stir Processing. *Ceram. Int.* **2020**, *46*, 20345–20356. [CrossRef]
15. Thoufiq Mohammed, K.; Manisekar, K. Mechanical and Dry Sliding Wear Behaviour of AZ31-TiO_2 and AZ31-TiO_2-Sn Metal Matrix Composites. *Int. J. Met.* **2022**, *17*, 1883–1898. [CrossRef]
16. Aydin, F.; Durgut, R. Estimation of Wear Performance of AZ91 Alloy under Dry Sliding Conditions Using Machine Learning Methods. *Trans. Nonferrous Met. Soc. China (Engl. Ed.)* **2021**, *31*, 125–137. [CrossRef]
17. Kaviti, R.V.P.; Jeyasimman, D.; S C, R.K.; Babu, M. Investigation of Wear Behaviour of Magnesium Reinforced with Boron Nitride Nanocomposite Using ANN. *J. Mines Met. Fuels* **2022**, *69*, 190. [CrossRef]
18. Kruthiventi, S.S.H.; Ammisetti, D.K. Experimental Investigation and Machine Learning Modeling of Wear Characteristics of AZ91 Composites. *ASME J. Tribol.* **2023**, *145*, 101704. [CrossRef]
19. Yu, S.R.; Huang, Z.Q. Dry Sliding Wear Behavior of Fly Ash Cenosphere/AZ91D Mg Alloy Composites. *J. Mater. Eng. Perform.* **2014**, *23*, 3480–3488. [CrossRef]
20. Xiu, K.; Wang, H.Y.; Sui, H.L.; Wang, Y.; Xu, C.L.; Wang, J.G.; Jiang, Q.C. The Sliding Wear Behavior of TiC_p/AZ91 Magnesium Matrix Composites. *J. Mater. Sci.* **2006**, *41*, 7052–7058. [CrossRef]
21. Ammisetti, D.K.; Kruthiventi, S.S.H. Experimental Investigation of the Influence of Various Wear Parameters on the Tribological Characteristics of AZ91 Hybrid Composites and Their Machine Learning Modeling. *ASME J. Tribol.* **2024**, *146*, 051704. [CrossRef]

22. Vignesh, R.V.; Padmanaban, R. Forecasting Tribological Properties of Wrought AZ91D Magnesium Alloy Using Soft Computing Model. *Russ. J. Non-Ferrous Met.* **2018**, *59*, 135–141. [CrossRef]
23. Hasan, M.S.; Kordijazi, A.; Rohatgi, P.K.; Nosonovsky, M. Triboinformatics Approach for Friction and Wear Prediction of Al-Graphite Composites Using Machine Learning Methods. *J. Tribol.* **2022**, *144*, 011701. [CrossRef]
24. Chicco, D.; Warrens, M.J.; Jurman, G. The Coefficient of Determination R-Squared Is More Informative than SMAPE, MAE, MAPE, MSE and RMSE in Regression Analysis Evaluation. *PeerJ Comput. Sci.* **2021**, *7*, e623. [CrossRef] [PubMed]
25. Alagarsamy, S.V.; Balasundaram, R.; Ravichandran, M.; Mohanavel, V.; Karthick, A.; Devi, S.S. Taguchi Approach and Decision Tree Algorithm for Prediction of Wear Rate in Zinc Oxide-Filled AA7075 Matrix Composites. *Surf. Topogr. Metrol. Prop.* **2021**, *9*, 035005. [CrossRef]

Disclaimer/Publisher's Note: The statements, opinions and data contained in all publications are solely those of the individual author(s) and contributor(s) and not of MDPI and/or the editor(s). MDPI and/or the editor(s) disclaim responsibility for any injury to people or property resulting from any ideas, methods, instructions or products referred to in the content.